THE JOURNAL OF PHYSICAL CHEMISTRY B

 VOLUME 108, NUMBER 32, AUGUST 12, 2004

LETTERS

Molecular Dynamics Simulation of Ionic Liquids: The Effect of Electronic Polarizability

Tianying Yan,[†] Christian J. Burnham,[†] Mario G. Del Pópolo,[‡] and Gregory A. Voth*,[†]

Department of Chemistry and Henry Eyring Center for Theoretical Chemistry, University of Utah, Salt Lake City, Utah 84112-0850, and Atomistic Simulation Group, School of Mathematics and Physics, Queen's University Belfast, Belfast BT7 1NN, Northern Ireland

Received: June 2, 2004; In Final Form: June 30, 2004

An electronically polarizable model has been developed for the ionic liquid 1-ethyl-3-methylimidazolium nitrate ($EMIM^+/NO_3^-$). Molecular dynamics simulation studies were then performed on both the polarizable and nonpolarizable versions of the model. Comparisons of shear viscosity and diffusion constants at 400 K show that the effects of polarizability are quite substantial and the polarizable model results are in better agreement with the experimental values.

Room temperature molten salts (RTMS), or ionic liquids (ILs), have recently stimulated a significant body of research. Like inorganic molten salts, ILs are composed solely of ions, but in contrast their melting point is often less than 100 °C.[1] There are potentially on the order of 10^5 varieries of ILs, but most ILs of recent interest are based on nitrogen-rich alkyl-substituted heterocyclic cations, accompanied by different inorganic anions. Despite the current level of research activity, many of the properties of these interesting liquids remain to be elucidated.[2]

The focus of attention in this letter is the effect of electronic polarizability on the dynamics of ILs. We shall study the specific IL system 1-ethyl-3-methylimidazolium nitrate ($EMIM^+/NO_3^-$), in which both $EMIM^+$ and NO_3^- are polarizable and anisotropic,[3] making it highly desirable to model these interactions using a fully polarizable force field despite the additional CPU cost incurred.[4] Though the viscosities of various ILs have been measured experimentally,[5] the computer simulation of viscosity has not yet been reported to our knowledge. Although calculations of the diffusion constant have been attempted,[6−8] it is found that the simulated diffusion constants, obtained by nonpolarizable IL models, are likely lower than the experimental measurements. Therefore, it is of considerable interest to see if the apparent deficiencies of these models can be improved by the use of a polarizable force field. In this study, we present the shear viscosity and diffusion constant of $EMIM^+/NO_3^-$ obtained by computer simulation for both polarizable and nonpolarizable models, and these results are compared with experimental measurements.

The nonpolarizable force field model in this work has the standard form. The force field parameters were taken from our previous study,[8] and the partial charges were taken by fitting the MP2/6−31g* electrostatic potential with the RESP charge model.[9] The force field parameters and partial charges are available as Supporting Information. For the present polarizable model, we adopt the modified dipole tensor method of Thole,[10] in which both atomic and (anisotropic) molecular polarizabilities can be reasonably described through the use of a "smeared" dipole−dipole interaction. We parameterized the model to ab initio MP2/cc-pVTZ(-f)[11] molecular polarizabilities, based on the MP2/6−31g* optimized structure, for each atom. Specifi-

* Corresponding author. E-mail: voth@chem.utah.edu.
[†] University of Utah.
[‡] Queen's University Belfast.

10.1021/jp047619y CCC: $27.50
Published on Web 07/17/2004

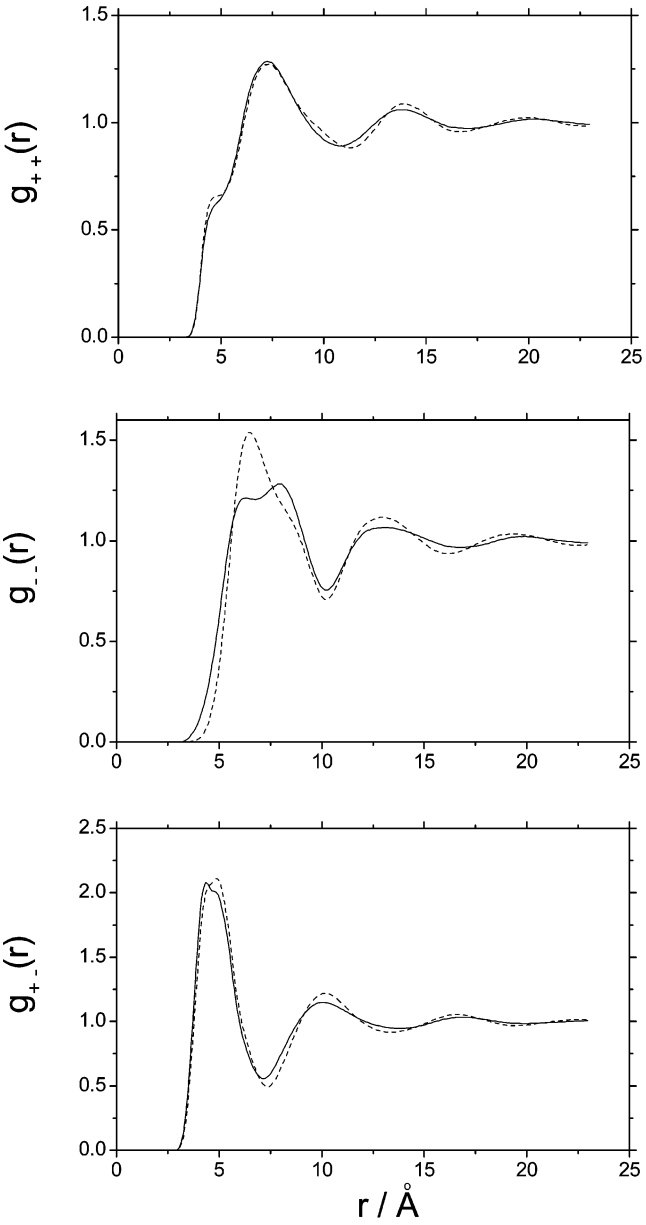

Figure 1. The center-of-mass partial radial distribution functions (PRDF) for the cation−cation $g_{++}(r)$, anion−anion $g_{--}(r)$, and cation−anion $g_{+-}(r)$. Polarizable model (solid line); nonpolarizable model (dashed line).

cally, the atomic polarizabilities for $EMIM^+$ are 0.370 Å^3 for H, 1.183 Å^3 for C, and 1.367 Å^3 for N, while for NO_3^- they are 0.755 Å^3 for N and 1.479 Å^3 for O. The Thole smearing function takes the form $\rho^f(r_{ij}) = (a^3/8\pi)\exp[-ar_{ij}/(\alpha_i\alpha_j)^{1/6}]$, where α_i and α_j are the atomic polarizabilities of atom i and j, and the smearing factor is $a = 1.225$.

The present parameterization is able to reproduce the MP2/cc-pVTZ(-f)//MP2/6−31g* isotropic molecular polarizabilities. In particular, at the MP2/6−31g* optimized geometry we obtain values of 11.29 Å^3 for $EMIM^+$ and 3.41 Å^3 for NO_3^-, compared to the electronic structure values of 11.43 Å^3 for $EMIM^+$ and 3.33 Å^3 for NO_3^-. The details for developing the polarizable IL model will be reported later,[12] but the present implementation is based on that of Burnham et al.[13] The resulting polarizable force-field was implemented in the DL_POLY 2.13[14] molecular dynamics (MD) package and parallelized with the replicated data method.[15]

For both the polarizable and nonpolarizable models, the IL MD simulation consisted of 400 $EMIM^+/NO_3^-$ ion pairs (9200 atoms) with an all-atom, all-flexible model. Periodic boundary conditions (PBC) were employed with a cubic cell, and the long-range charge−charge, charge−dipole, and dipole−dipole interactions were treated using the Ewald sum.[16] The induced dipoles were propagated using an extended Lagrangian method,[17] including a Nóse-Hoover thermostat[18] to keep the dipoles at 0.1 K, close to their minimized adiabatic surface.[19] The integration time step was 0.5 fs and the total energy drift was found to be −0.0004% per ps for the polarizable model, while it was negligible for the nonpolarizable model. After a 500 ps constant NPT[20] equilibration for 400 K and 1 atm, the equilibrated densities were 1.177 g/cm^3 for the polarizable model and 1.174 g/cm^3 for the nonpolarizable model, which only differ by 0.3%. The systems were further equilibrated for 300 ps with a constant NVT[18] calculation at 400 K, followed by a 1.2 ns constant NVT production run with the phase space data (velocities and coordinates) recorded every 5 fs.

The center-of-mass partial radial distribution functions (PRDFs) of cation−cation $g_{++}(r)$, anion−anion $g_{--}(r)$, and cation−anion $g_{+-}(r)$, for both the polarizable and nonpolarizable models, are shown in Figure 1. A distinct feature from Figure 1 is that they exhibit very long-range spatial correlations, and the oscillation extends to 23 Å, which is about the half-length of the simulation box. The first maximum of $g_{++}(r)$ is much broader and weaker than that of $g_{+-}(r)$, in agreement with experimental measurement of a slightly different IL system $DMIM^+/Cl^-$.[21] This is expected because the IL ions are quite bulky, and as a result the first coordinate shells of cation−cation and anion−anion are well beyond 10 Å and for cation−anion it is above 7 Å. It is of interest to note that the small "bump" at about 4.5 Å in $g_{++}(r)$ was also observed in the above experiment, where it occurs at about 4 Å, partly due to the fact that the size of $DMIM^+$ is smaller than $EMIM^+$. The occurrence of the small "bump" in $g_{++}(r)$ may be caused by the orientational correlation in the cation−cation spatial arrangement.[12]

The effect of electronic polarization on the structure can be seen by comparing the polarizable model with the nonpolarizable model. As shown in Figure 1, the first maxima of the PRDFs are shifted to the shorter distance and bring the ions in closer contact with each other for the polarizable model. As electronic polarization is allowed, an additional screening effect is switched on to reduce the Coulombic repulsion for $g_{++}(r)$ and $g_{--}(r)$, as well as to reduce the van der Waals short-range repulsion for $g_{+-}(r)$. Though the simulations with polarizable and nonpolarizable models were both run on the same temperature, the effect of using a polarizable model appears similar to running the nonpolarizable model at a higher temperature, an effect which has been previously observed by Ribeiro.[22]

The big difference is seen on $g_{--}(r)$, and a detailed analysis will be given later.[12] Briefly, this may be explained by the induction effect when the polarizability is allowed. Since the polarizability of NO_3^- is about 1/3 of that of $EMIM^+$, the spatial arrangement of the NO_3^- seems to be in a way that helps maximizing the local electric field on $EMIM^+$. Similar effects were also observed in a simulation study of inorganic molten salt $ZnCl_2$,[23] in which Zn^{2+} were spatially rearranged to maximize the local electric field on Cl^-. In both cases, PRDFs of the less polarizable ion are seen to be much influenced as polarizability is switched on.

The dynamics of density fluctuation was also analyzed for both IL models. Figure 2 shows the transverse current correlation

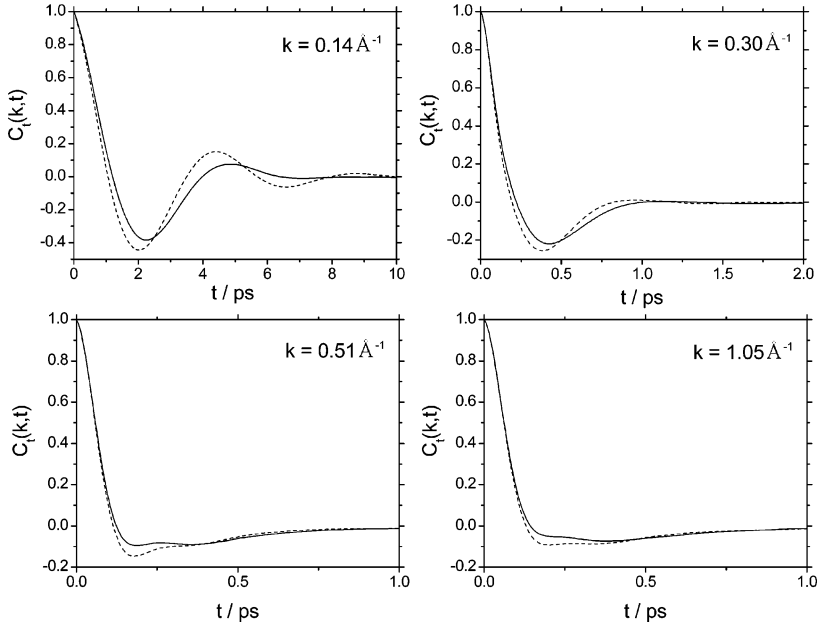

Figure 2. Four selected normalized transverse current correlation functions $C_t(k,t)$ of both the polarizable model (solid line) and the nonpolarizable model (dashed line).

function, $C_t(k,t)$, at four selected wave vectors for the two models. The normalized transverse current correlation function is defined as

$$C_t(k,t) = \frac{\langle \boldsymbol{J}_t(\boldsymbol{k},t)\boldsymbol{J}_t(-\boldsymbol{k},0)\rangle}{\langle \boldsymbol{J}_t(\boldsymbol{k},0)\boldsymbol{J}_t(-\boldsymbol{k},0)\rangle} \tag{1}$$

where $\boldsymbol{J}_t(\boldsymbol{k},t)$ is the total transverse current operator. For a binary liquid, $\boldsymbol{J}_t(\boldsymbol{k},t)$ is given by[24] $\boldsymbol{J}_t(\boldsymbol{k},t) = 1/(\sqrt{N})\sum_{i=1}^{N}\hat{\boldsymbol{k}} \times m_i \mathrm{v}_i(t) \exp[i\boldsymbol{k}\boldsymbol{r}_i(t)]$, where m_i, $\boldsymbol{v}_i$, and $\boldsymbol{r}_i$ are the mass, center-of-mass velocity, and position of the ith ion, respectively, and $k = |\boldsymbol{k}|$ are the wave vectors of the same modulus. The value $k = 0.14$ Å^{-1} is the smallest wave vector allowed by the PBC cell. Comparing $C_t(k,t)$ of the same wave vectors for both models, especially at lower k, it is seen that the negative minimum in $C_t(k,t)$ of the polarizable model is shallower and occurs at a later time than in the nonpolarizable model, which is an indication of the lower viscosity in the polarizable model.

The viscous flow in a fluid is described by $C_t(k,t)$ which contains the long-time and large-distance behavior. The Navier−Stokes equation gives a single-exponential decay for the TCF at low wave vector and long time.[25] The deviation from such behavior, as seen in Figure 2, can be generalized within a viscoelastic theory through a memory function model,[26,27] $\mathrm{d}C_t(k,t)/\mathrm{d}t = -\int_0^t \mathrm{d}t' M_t(k,t-t')C_t(k,t')$. Here we adopt the memory function $M_t(k,t)$ of the following form

$$M_t(k,t) = \omega_t^2[(1-\alpha_k)\exp(-\pi t^2/4\tau_{1k}^2) + \alpha_k \exp(-t/\tau_{2k})] \tag{2}$$

where the second frequency moment[26] of $C_t(k,t)$, $\omega_t^2 = \{\langle|\dot{\boldsymbol{J}}_t(k,t)|^2\rangle\}/\{\langle|\boldsymbol{J}_t(k,0)|^2\rangle\}$, can be calculated by taking the numerical derivatives of the transverse current, $\boldsymbol{J}_t(\boldsymbol{k},t)$, from MD simulation. The first part of eq 2 is a Gaussian term which takes into account the short-time ballistic collisions when the dynamic variables lose memory rapidly, while the second part represents the long-time collective effects. Equation 2 has three parameters, α_k, τ_{1k}, and τ_{2k}, which can be determined by fitting the spectrum of $C_t(k,t)$, i.e.,

$$C_t(k,\omega) = \frac{2M_t'(k,\omega)}{[\omega - M_t''(k,\omega)]^2 + M_t'(k,\omega)^2} \tag{3}$$

where $C_t(k,\omega) = \int_{-\infty}^{\infty} \mathrm{d}t\, e^{-i\omega t}C_t(k,t)$ is the Fourier transform of $C_t(k,t)$ and

$$M_t'(k,\omega) = \omega_t^2\left[(1-\alpha_k)\tau_{1k}\exp(-\tau_{1k}^2\omega^2/\pi) + \frac{\alpha_k/\tau_{2k}}{\omega^2 + (1/\tau_{2k}^2)}\right]$$

$$M_t''(k,\omega) = \omega_t^2\left[(1-\alpha_k)\tau_{1k}\exp(-\tau_{1k}^2\omega^2/\pi)\,\mathrm{erf}\, i(\tau_{1k}\omega/\pi^{1/2}) + \frac{\alpha_k\omega}{\omega^2 + 1/\tau_{2k}^2}\right]$$

are the real and imaginary parts of the Laplace transform of $M(k,t)$, respectively. In the above expression, $\mathrm{erf}\, i(\tau_{1k}\omega/\pi^{1/2}) = \mathrm{erf}(i\tau_{1k}\omega/\pi^{1/2})/i = (2/\pi^{1/2})\int_0^{\tau_{1k}\omega/\pi^{1/2}} \exp(y^2)\,\mathrm{d}y$ is the imaginary error function and $\exp(-\tau_{1k}^2\omega^2/\pi)\int_0^{\tau_{1k}\omega/\pi^{1/2}} \exp(y^2)\,\mathrm{d}y$ is Dawson's integral.[28]

Figure 3 shows $C_t(k,\omega)$, obtained by Fourier transform of $C_t(k,t)$ from MD simulation, as well as by the fitting given in eq 3, for the four wave vectors in Figure 2 for both models. The spectrum of $C_t(k,t)$ provides information on the system response with respect to a wave vector k and frequency ω. As $k \to 0$, $C_t(k,t)$ will be overdamped because the liquid is unable to support shear waves of long wavelength. The occurrence of the nonzero peak in $C_t(k,\omega)$, even at $k = 0.14$ Å^{-1}, indicates the system is considerably rigid, similar to the hydrogen bonding network in water.[29] The nonzero tail at large frequency for larger wave vectors is caused by noise. As $k \geq 0.51$ Å^{-1} there is a shoulder in $C_t(k,\omega)$ between 20 and 30 ps^{-1}, which reveals the single-particle motion, as compared to lower wave vectors,

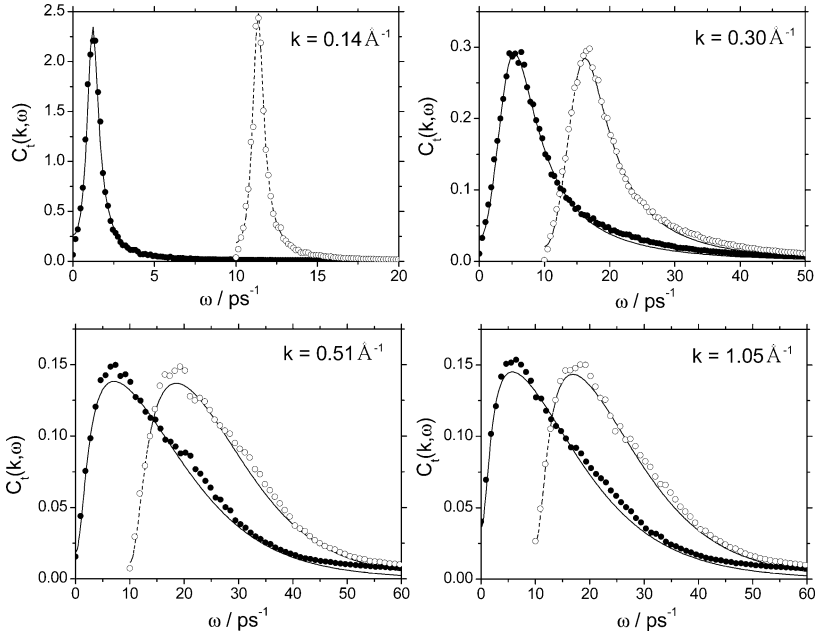

Figure 3. Fourier transform normalized transverse current correlation function $C_t(k,\omega)$ obtained from MD simulation as well as the fit by eq 3. Solid circles are the discrete Fourier transform of $C_t(k,t)$ for the polarizable model; solid line is the fitted $C_t(k,\omega)$, with eq 3 utilizing the memory function proposed in eq 2, for the polarizable model; open circles are the discrete Fourier transform of $C_t(k,t)$ for the nonpolarizable model; dashed line is the fitted $C_t(k,\omega)$ for the nonpolarizable model. $C_t(k,\omega)$s of the nonpolarizable model are horizontally offset by 10 ps^{-1} on the *x*-axis.

which are associated with collective motion. Overall, the memory function, eq 3, fits $C_t(k,\omega)$ quite adequately. The fitted parameters are available as Supporting Information.

The wave vector dependent shear viscosities, using the parameters α_k, τ_{1k}, and τ_{2k} obtained from the fitting in Figure 3, are given by

$$\eta(k) = \lim_{z\to 0} \frac{\rho}{k^2}\tilde{M}_t(k,z) = \frac{\rho}{k^2}\tilde{M}_t(k,0) \qquad (4)$$

where ρ is the mass density and $\tilde{M}_t(k,0)$ is given by the zero frequency value of eq 3. Extrapolating the above expression to the $k \to 0$ limit gives the hydrodynamic value of the shear viscosity, i.e., $\eta = \lim_{k\to 0}\lim_{z\to 0}(\rho/k^2)\tilde{M}_t(k,z)$. An extrapolation of the small k dependent viscosity may be written as[30] $\eta(k)/\eta \approx (1 + a^2k^2)^{-1}$,where η is the approximated $k \to 0$ limited shear viscosity. As shown in Figure 4, the extrapolation to the zero k shear viscosity is 4.74 c.p. for the polarizable model and 6.84 c.p. for the nonpolarizable model. Therefore, electronic polarization effects are seen to *decrease* the system viscosity. It is also of interest to note that the inclusion of polarizability brings the shear viscosity into much closer agreement with the experimental result at 400 K of 4.42 c.p.[5]

Figure 5 shows the mean square displacement (MSD), in a log−log plot up to 1 ns, of $EMIM^+$ and NO_3^- for both models. Remarkably, the slope of the MSD of the polarizable model is more than three times larger than the nonpolarizable model by 1 ns. The short time inertial motion ($\langle\Delta r(t)^2\rangle \propto t^2$) due to the ballistic collisions lasts less than 0.1 ps, followed by a long time intermediate region (∼100 ps for the polarizable model and ∼800 ps for the nonpolarizable model), which finally goes to linear diffusion ($\langle\Delta r(t)^2\rangle \propto t$).[8] A linear fit to the MSD between 900 and 1000 ps and using the Einstein relation, $\langle\Delta r(t)^2\rangle = 6\Delta t$, gives the diffusion constants 1.49×10^{-10} m^2/s and 1.55×10^{-10} m^2/s for $EMIM^+$ and NO_3^-, respectively, for the polarizable model, and 5.07×10^{-11} m^2/s and 4.80×10^{-11} m^2/s for $EMIM^+$ and NO_3^-, respectively, for the nonpolarizable model. For the nonpolarizable model, the local charge neutrality

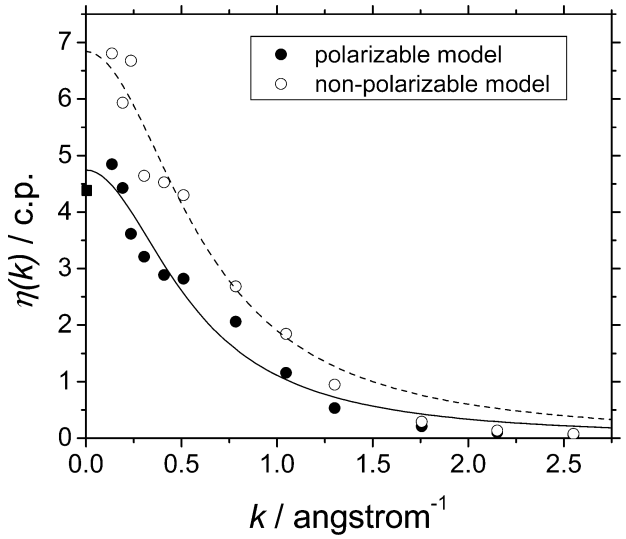

Figure 4. The wave vector dependent shear viscosity $\eta(k)$ calculated by eq 4 at different values of k. Solid line is the fitted $\eta(k)$ of the polarizable model; dashed line is the fitted $\eta(k)$ of the nonpolarizable (see text). The solid square denotes the experimental shear viscosity at 400 K.[5]

around a diffusing ion can be maintained only by translation of its neighbors, but when polarization is allowed, an additional screening mechanism is present that does not entail the movement of ion cores. The net result is that the cage effect is smaller for polarizable ions, which leads to a larger diffusion constant.[24] Our simulation at 400 K shows that diffusion constant of the polarizable model is three times of the nonpolarizable model.

In this preliminary study, a polarizable model for the ionic liquid, 1-ethyl-3-methylimidazolium nitrate ($EMIM^+/NO_3^-$) has been presented and studied by MD simulation. The memory function in eq 2 gives a reasonable fit to the spectrum of the normalized transverse current correlation function $C_t(k,t)$. A comparison between the polarizable and nonpolarizable models shows that the polarizable model yields a shear viscosity in much

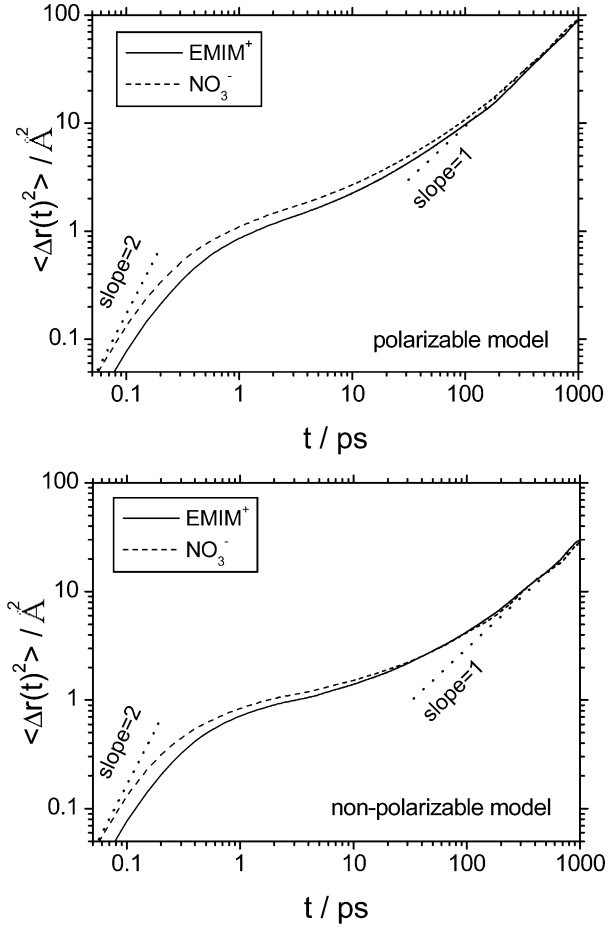

Figure 5. Mean-squared displacements of $EMIM^+$ and NO_3^- for the polarizable model (upper panel) and the nonpolarizable model (lower panel). Solid line is for $EMIM^+$; dashed line is for NO_3^-; and the dotted straight line with slope = 1 and slope = 2 are guides for the eye.

better agreement with the experimental result. The main effect of the electronic polarizability is to make the ions more mobile. This effect results in a lower viscosity and significantly higher diffusion constant. The present study reveals that the inclusion of electronic polarizability can considerably improve the agreement between simulation and experiment for IL systems.

Acknowledgment. This study is supported by Air Force Office of Scientific Research (FA9550-04-1-0381). The authors thank Dr. Gary Ayton, Dr. Jonggu Jeon, and Dr. Feng Wang for many helpful discussions. An allocation of supercomputing time at the National Center for Supercomputing Applications (NCSA) is gratefully acknowledged.

Supporting Information Available: Force field parameters and partial charges. This material is available free of charge via the Internet at http://pubs.acs.org.

References and Notes

(1) Welton, T. *Chem. Rev.* **1999**, *99*, 2071.
(2) Rogers, R. D.; Seddon, K. R. *Science* **2003**, *302*, 792.
(3) Cang, H.; Li, J.; Fayer, M. D. *J. Chem. Phys.* **2003**, *119*, 13017.
(4) Gray-Weale, A.; Madden, P. A. *Mol. Phys.* **2003**, *101*, 1761.
(5) Seddon, K. R.; Stark, A.; Torres, M.-J. In *Clean Solvents: Alternative Media for Chemical Reactions and Processing*; Abraham, M., Moens, L., Eds.; ACS Symposium Series 819; Americal Chemical Society: Washington, DC, 2002.
(6) Margulis, C. J.; Stern, H. A.; Berne, B. J. *J. Phys. Chem. B* **2002**, *106*, 12017.
(7) Morrow, T. I.; Maginn, E. J. *J. Phys. Chem. B* **2003**, *106*, 12807.
(8) Del Pópolo, M. G.; Voth, G. A. *J. Phys. Chem. B* **2004**, *108*, 1744.
(9) Bayly, C. I.; Cieplak, P.; Cornell, W. D.; Kollman, P. A. *J. Phys. Chem.* **1993**, *97*, 10269.
(10) Thole, B. T. *Chem. Phys.* **1981**, *59*, 341.
(11) Beachy, M. D.; Chasman, D.; Murphy, R. B.; Halgren, T. A.; Friensner, R. A. *J. Am. Chem. Soc.* **1997**, *119*, 5908.
(12) Yan, T.; Burnham, C. J.; Voth, G. A., manuscript in preparation.
(13) Burnham, C. J.; Li, J.; Xantheas, S. S. *J. Chem. Phys.* **1999**, *110*, 4566.
(14) Smith, W.; Forester, T. R. The DL_POLY Molecular Simulation Package; http://www.dl.ac.uk/TCSC/Software/DL_POLY/main.html, 1999.
(15) Smith, W. *Comput. Phys. Commun.* **1992**, *67*, 392.
(16) Smith, W. *CCP5 Information Quarterly* **1982**, *4*, 13.
(17) Saboungi, M.-L.; Rahman, A.; Halley, J. W.; Blander, M. *J. Chem. Phys.* **1988**, *88*, 5818.
(18) Hoover, W. G. *Phys. Rev. A* **1985**, *31*, 1695.
(19) Sprik, M. *J. Phys. Chem.* **1991**, *95*, 2283.
(20) Melchionna, P.; Cicocoti, G.; Holian, B. *Mol. Phys.* **1993**, *78*, 533.
(21) Hardacre, C.; Holbrey, J. D.; Jane McMath, S. E.; Bowron, D. T.; Soper, A. K. *J. Chem. Phys.* **2003**, *118*, 273.
(22) Ribeiro, M. C. C. *J. Phys. Chem. B* **2003**, *107*, 9520.
(23) Madden, P. A.; Wilson, M. *J. Phys.: Condens. Matter* **2000**, *12*, A95.
(24) Hansen, J.-P.; McDonald, I. R. *The Theory of Simple Liquids*, 2nd ed.; Academic Press: San Diego, 1986.
(25) Boon, J. P.; Yip, S. *Molecular Hydrodyamics*; Dover: New York, 1991.
(26) Ailawadi, N. K.; Rahman, A.; Zwanzig, R. *Phys. Rev. A* **1971**, *4*, 1616.
(27) Levesque, D.; Verlet, L.; Kurkijarvi, J. *Phys. Rev. A* **1973**, *7*, 1690.
(28) Press, W. H.; Teukolsky, S. A.; Vetterling, W. T.; Flannery, B. P. *Numerical Recipes in Fortran*; Cambridge University Press: 1992.
(29) Rahman, A.; Stillinger, F. H. *Phys. Rev. A* **1974**, *10*, 368.
(30) Alley, W. E.; Alder, B. J. *Phys. Rev. A* **1983**, *27*, 3158.